CONDENSED MATTER PHYSICS

Evidence for solitonic spin excitations from a charge-lattice–coupled ferroelectric order

K. Sunami[1]*, T. Nishikawa[1], K. Miyagawa[1], S. Horiuchi[2], R. Kato[3], T. Miyamoto[4], H. Okamoto[4,5], K. Kanoda[1]*

Copyright © 2018 The Authors, some rights reserved; exclusive licensee American Association for the Advancement of Science. No claim to original U.S. Government Works. Distributed under a Creative Commons Attribution NonCommercial License 4.0 (CC BY-NC).

Topological defects have been explored in different fields ranging from condensed matter physics and particle physics to cosmology. In condensed matter, strong coupling between charge, spin, and lattice degrees of freedom brings about emergent excitations with topological characteristics at low energies. One-dimensional (1D) systems with degenerate dimerization patterns are typical stages for the generation of topological defects, dubbed "solitons"; for instance, charged solitons are responsible for high electrical conductivity in doped *trans*-polyacetylene. Here, we provide evidence based on a nuclear magnetic resonance (NMR) study for mobile spin solitons deconfined from a strongly charge-lattice–coupled spin-singlet ferroelectric order in a quasi-1D organic charge-transfer complex. The NMR spectral shift and relaxation rate associated with static and dynamic spin susceptibilities indicate that the ferroelectric order is violated by dilute solitonic spin excitations, which were further demonstrated to move diffusively by the frequency dependence of the relaxation rate. The traveling solitons revealed here may promise the emergence of anomalous electrical and thermal transport.

INTRODUCTION

One-dimensional (1D) electron-lattice–coupled systems exhibit various instabilities followed by lattice symmetry breaking; Peierls and spin-Peierls instabilities are well-known examples (*1*, *2*). In these systems, topological defects, which are exotic excitations emerging in diverse physical systems (*3*), are expected to be generated (*4*, *5*). The organic complex, tetrathiafulvalene-*p*-chloranil (TTF-CA), in which the donor molecule, TTF, and the acceptor molecule, CA, stack alternately to form 1D columns (Fig. 1A), shows charge-transfer and lattice-dimerization instabilities. At ambient pressure and temperature, TTF-CA is in a quasi-neutral (*N*) state (the degree of charge transfer $\rho \sim 0.3$), with both TTF and CA forming electronic closed shells; upon cooling, TTF-CA transitions to a quasi-ionic (*I*) state ($\rho \sim 0.6$ to 0.7), with a collective electron transferred from TTF to CA to gain electrostatic energy at 81 K (*6*, *7*). The charge transfer is followed by simultaneous lattice dimerization (*8*–*10*), yielding an "electronic ferroelectricity" (*11*). Thus, TTF-CA is nonmagnetic in both the *N* phase (due to the closed-shell structure) and the dimerized *I* phase (due to spin-singlet pairing). As seen in Fig. 1B, dimerization can occur with one of two degenerate patterns (labeled I_A and I_B in Fig. 1B), leading to the emergence of solitonic spins as topological defects against long-range dimerization order. To date, these defects have been observed as frozen defects in 3D long-ranged dimerized ferroelectric order but not as topological thermal excitations (*12*, *13*).

The simultaneous charge-transfer and dimerization transition occur at an elevated temperature as the pressure is increased (*14*, *15*). However, a recent nuclear quadrupole resonance (NQR) study revealed that the charge transfer and dimerization are separated above ~8 kbar (*14*–*16*); the charge-transfer temperature continues to increase, whereas the dimerization transition temperature turns downward with increasing pressure (Fig. 1C) (*16*), suggesting a paraelectric *I* phase without static lattice dimerization in the region between the charge-transfer and dimerization lines (labeled I_{para} in Fig. 1C). Naively, the substantially charge-transferred I_{para} phase should carry paramagnetic spins on uniform 1D chains free from dimerization. An infrared spectroscopy study, however, found the activation of the a_g mode in CA molecules, indicative of lattice dimerization, at pressures above 8 kbar at ambient temperature (*17*, *18*). These contradicting results suggest that the dimerization is temporally fluctuating at a characteristic frequency in between the frequency windows of the NQR (10^7 Hz) and infrared (10^{12} Hz) probes (*16*). Thus, the I_{para} phase above 8 kbar is expected to host no homogeneous 1D spin chains but carry mobile solitonic spins that emerge at thermally activated topological boundaries separating oppositely polarized dimer domains. The purpose of the present work is to demonstrate the existence of topological magnetic excitations from a ferroelectric order for the first time, using nuclear magnetic resonance (NMR), which probes the spin states in a microscopic manner.

RESULTS AND DISCUSSION

Magnetic excitations investigated by ^{1}H-NMR and ^{13}C-NMR

NMR experiments were carried out for the ^{1}H and ^{13}C sites in TTF molecules (see Materials and Methods). First, to reveal the profile of the magnetic excitations in the pressure-temperature (*P*-*T*) phase diagram, we measured the ^{1}H-NMR spin-lattice relaxation rate, $^1T_1^{-1}$, which probes electron spin fluctuations, under various temperatures and pressures. At ambient temperature, $^1T_1^{-1}$ is vanishingly small in the *N* phase at low pressures, indicative of a nonmagnetic state, in agreement with the previous ^{1}H-NMR results (*19*, *20*), whereas it is rapidly enhanced with increased pressure above 8 kbar (Fig. 1B), at which point charge transfer is sharply promoted (Fig. 2B) (*16*, *21*). Even in the high-pressure region, however, $^1T_1^{-1}$ rapidly decreases on cooling (Fig. 2A). The contour plot of $^1T_1^{-1}$ in the *P*-*T* plane (Fig. 1C) shows that the area of active spin excitations nearly coincides with the I_{para} region (*16*), indicating that the I_{para} phase contains active spins, in contrast to the *N* phase and ferroelectric *I* (I_{ferro}) phase. The

[1]Department of Applied Physics, University of Tokyo, Bunkyo-ku, Tokyo 113-8656, Japan. [2]Flexible Electronics Research Center (FLEC), National Institute of Advanced Industrial Science and Technology (AIST), Tsukuba, Ibaraki 305-8565, Japan. [3]Condensed Molecular Materials Laboratory, RIKEN, Wako, Saitama 351-0198, Japan. [4]Department of Advanced Materials Science, University of Tokyo, Kashiwa, Chiba 277-8561, Japan. [5]AIST-UTokyo Advanced Operando-Measurement Technology Open Innovation Laboratory (OPERANDO-OIL), National Institute of AIST, Chiba 277-8568, Japan.
*Corresponding author. Email: sunami@mdf2.t.u-tokyo.ac.jp (K.S.); kanoda@ap.t.u-tokyo.ac.jp (K.K.)

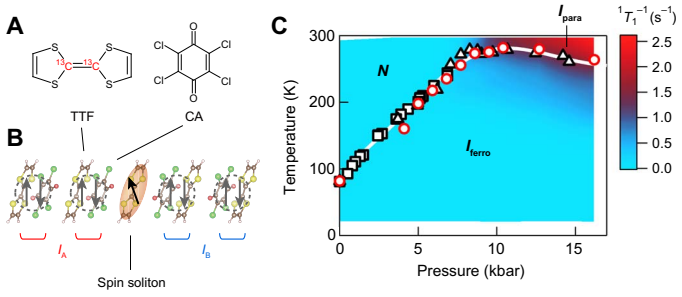

Fig. 1. Soliton excitation and phase diagram for TTF-CA. (**A**) Molecular structures of the TTF and CA molecules. The central double-bonded carbon atoms in the TTF molecule are substituted by ^{13}C isotopes for ^{13}C-NMR measurements. (**B**) Schematic of degenerate spin-singlet dimer patterns (I_A and I_B) in the quasi-ionic phase. A spin soliton with spin 1/2 emerges between them. (**C**) A contour plot of the ^{1}H-NMR spin-lattice relaxation rate, $^1T_1^{-1}$, in the pressure-temperature (*P-T*) plane of TTF-CA. The red circles indicate peak or kink temperatures for $^1T_1^{-1}$. The white squares and triangles indicate the dimerization transition temperatures as determined by previous neutron and NQR measurements, respectively (*14*, *16*).

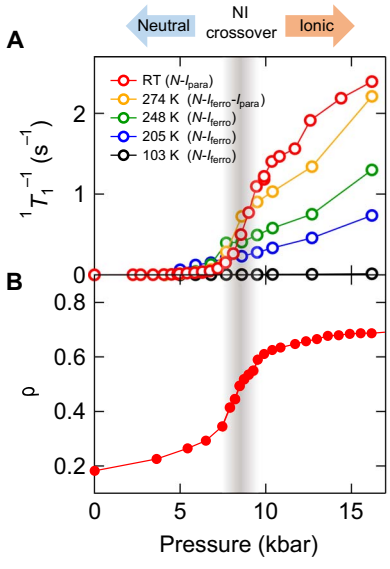

Fig. 2. ^{1}H-NMR relaxation rate and degree of charge transfer. (**A** and **B**) Pressure dependence of the ^{1}H-NMR spin-lattice relaxation rate, $^1T_1^{-1}$, under various temperatures (A) and the degree of charge transfer, ρ, evaluated by a previous NQR measurement (*16*) at room temperature (RT) (B). The gray line indicates the NI crossover pressure (defined as ρ = 0.5) at room temperature.

dimerization transition temperatures determined by $^1T_1^{-1}$ nearly reproduce the previous neutron scattering and ^{35}Cl-NQR results (*14*, *16*) except for 4.5 kbar, at which the pressure is possibly reduced because of the solidification of the pressure medium.

Next, we present ^{13}C-NMR results, which reveal that the active spins are solitonic instead of emerging on every TTF site. The ^{13}C nuclei residing on the central double-bonded carbon sites in TTF molecules (Fig. 1A) are more strongly hyperfine-coupled with electrons than ^{1}H nuclei located on the edges of TTF so that the NMR spin shift can be well resolved. The spectral shift could not be observed in the ^{1}H-NMR measurements (see the Supplementary Materials). Using the hyperfine coupling constant, we can quantitatively discuss the spin shift and relaxation rate involved with the static and dynamic spin susceptibilities, respectively, which provide key information for the nature of the magnetic excitations. Figure 3A shows the ^{13}C-NMR spectra measured under several different pressures at 285 K, where the system crosses over from the *N* phase to the I_{para} phase as pressure is increased. The spectra form two-peak structures due to dipolar coupling between adjacent ^{13}C nuclear spins at all pressures except for 3 kbar, at which the spectrum is disturbed by the appearance of the signal from the oil pressure medium because, at low pressures, the relaxation rate of the sample signal becomes long enough to be comparable to that of the oil signal. The spectral shift defined by the midpoint of the doublet is nearly independent of pressure up to 6 kbar and gradually increases with further pressure (Fig. 3B). In general, the spectral shift has two origins: the spin shift, δ_s, which originates from the hyperfine interaction with electron spins that is proportional to the local spin susceptibility at the ^{13}C site, and the chemical shift, σ, originating from the orbital motion of electrons. In the nonmagnetic *N* phase at low pressures, the spectral position is solely determined by the chemical shift, which yields ~82 parts per million (ppm); this value is unchanged even in the *I* state at high pressures, as indicated by the spectrum measured at 14 kbar and 144 K (Fig. 3A), at which the TTF-CA is in a nonmagnetic *I* state. The spin shift that appears at 6 kbar reaches 51 ppm at 14 kbar (Fig. 3B), and concomitantly, the ^{13}C spin-lattice relaxation rate $^{13}T_1^{-1}$ increases with pressure before leveling off to a value of approximately 11 s^{-1} (Fig. 3C), indicating the emergence of paramagnetic spins in the I_{para} phase, in agreement with the ^{1}H-NMR results. There appears to be an anomaly around 12 kbar in Figs. 2A (RT) and 3C; however, it is probably not intrinsic but due to statistic errors because such an anomaly was not observed in a separate sample (for details, see the Supplementary Materials).

We note that the previously reported ^{35}Cl-NQR relaxation rate, $^{35}T_1^{-1}$, shows a decrease with increasing pressure above 9 kbar (*16*), unlike the behavior of the NMR $^1T_1^{-1}$ and $^{13}T_1^{-1}$. This is because NQR probes lattice fluctuations, whereas NMR probes spin excitations. The lattice fluctuations are expected to be enhanced close to the dimerization transition temperature T_c, which decreases as pressure is increased above 9 kbar. Because room temperature departs further from T_c at higher pressures, lattice fluctuations at room temperature are gradually depressed under pressurization, as observed in (*16*).

δ_s is related to the spin susceptibility, χ, through the expression (*22*)

$$\delta_s = a_{||}\chi/\mu_B N_A \quad (1)$$

where N_A is the Avogadro constant, μ_B is the Bohr magneton, and $a_{||}$ is the hyperfine coupling component parallel to an external magnetic field, *H*. Using the $^{13}a_{||}$ value of 10.8 kOe/μ_B, the hyperfine coupling constant of the analogous material, $(TMTTF)_2X$ (X = Br and AsF_6) (*23*, *24*), because that of TTF-CA is not known, χ is estimated to be 2.6×10^{-5} emu/mol TTF at 14 kbar (Supplementary Materials), which is one or two orders of magnitude smaller than that of other organic quasi-1D spin systems [e.g., ~6×10^{-4} emu/mol spin in TTF-BA (*25*, *26*) and $(TMTTF)_2AsF_6$ (*24*) at room temperature]. If the value of 2.6×10^{-5} emu/mol for TTF is the low-temperature saturating value of spin susceptibility of the uniform 1D antiferromagnetic Heisenberg model (AFHM), the exchange interaction yields an unrealistically large value, *J* = 5900 K, referring to the theoretical calculations by Bonner and Fisher (*27*) and Estes *et al.* (*28*). On the other hand, we compare the experimental $^{13}T_1^{-1}$ values with the

consequence of the scaling theory for the uniform 1D AFHM, expressed as (*29*, *30*)

$$T_1^{-1} = a_\perp^2 D/\hbar J \quad (2)$$

where $a_\perp$ is the hyperfine coupling component perpendicular to H, $\hbar$ is the reduced Planck constant, and D is a nonuniversal constant giving the overall magnitude of the dynamical spin susceptibility. Using values of D = 0.15, as determined for Sr_2CuO_3 (*30*), which is an ideal 1D Heisenberg spin system, and $^{13}a_\perp$ = 5.6 kOe/μ_B (Supplementary Materials), the uniform 1D AFHM with J = 5900 K, which is obtained from the spin shift analysis, gives an estimate of $^{13}T_1^{-1}$ = 1.1 s^{-1} (Fig. 3D), which is one order of magnitude smaller than the experimental value of $^{13}T_1^{-1}$ = 11 s^{-1} at 14 kbar. Conversely, if we estimate the spin susceptibility expected from the experimental value of $^{13}T_1^{-1}$ = 11 s^{-1} in the 1D AFHM scenario, Eq. 2 yields the J value of 580 K, which gives the low-temperature spin susceptibility of 3.7 × 10^{-4} emu/mol TTF (Fig. 3D), more than an order of magnitude larger than the experimentally determined value of 2.6 × 10^{-5} emu/mol TTF. Thus, the experimental results of spin susceptibility and relaxation rate are mutually incompatible in the framework of the uniform 1D AFHM.

For reference, we also examine the compatibility of the experimental values χ and $^{13}T_1^{-1}$ of the putative 1D AFHM system, $(TMTTF)_2AsF_6$, in the similar analysis; in the low-temperature paramagnetic state at 80 K (*24*), χ = 4.2 × 10^{-4} emu/mol spin and $^{13}T_1^{-1}$ = 27.5 s^{-1}, which is the averaged value of $^{13}T_1^{-1}$ at the inner and outer carbons of the charge-rich TMTTF molecules. The 1D AFHM fitting of the χ data is reported to yield J = 410 K (*31*), which would result in $^{13}T_1^{-1}$ = 22 s^{-1} for the 1D AFHM, using the same D value of 0.15 and $^{13}a_\perp$ = 13 kOe/μ_B, in consideration of a spin-1/2 per TMTTF dimer (Supplementary Materials). The agreement between the experimental value, 27.5 s^{-1}, and the expected value, 22 s^{-1}, is excellent, demonstrating that the 1D AFHM works well for $(TMTTF)_2AsF_6$. At the same time, this analysis suggests that the D value of 0.15 is widely applicable to 1D AFHM systems including inorganic and organic materials. Thus, the contradiction between the experimental values and the 1D-AFHM expectations for TTF-CA suggests that the uniform 1D AFHM is not appropriate for describing the spin state in question, invoking an alternative picture. The extraordinarily small value of χ strongly suggests the presence of solitonic spin excitations. Assuming that the spin solitons behave similarly to Curie spins, the soliton density n is estimated to be ~0.02 spins per TTF or CA molecule at 285 K under 14 kbar. Compared with $n \sim 10^{-4}$ spins in the I_{ferro} phase at ambient pressure (*12*), many more spin solitons are thermally activated in the I_{para} phase. Both the spin shift and T_1^{-1} are sharply enhanced around the neutral-ionic (NI) boundary, whereas the degree of charge transfer is gradually increased even in the low-pressure region (Fig. 2B). These results imply that the soliton density is not proportional to the density or volume fraction of ionic domains, but the solitonic excitations require a certain amount of ionic domains that are thermally generated, and rapidly develop under further pressure. Then, the soliton density slightly increases with pressure in the I_{para} phase. The observed large value of $^{13}T_1^{-1}$ in the I_{para} phase is likely due to their traveling along the 1D chains, possibly explaining why $^{13}T_1^{-1}$ shows a somewhat different pressure dependence compared to the spin shift.

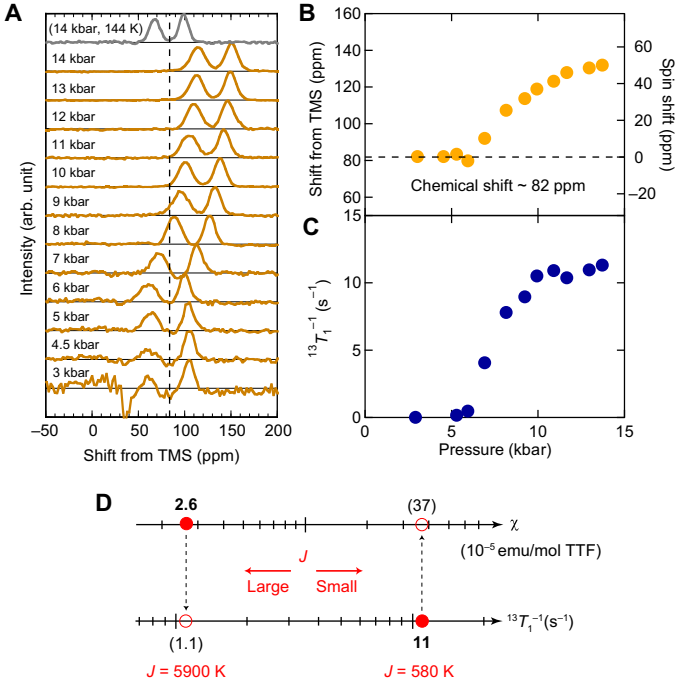

Fig. 3. ^{13}C-NMR spectral shift and relaxation rate. (**A**) Pressure dependence of ^{13}C-NMR spectra at 285 K (brown lines). The uppermost (gray) line shows a spectrum measured at 144 K under 14 kbar in the I_{ferro} phase. The origin of the horizontal axis corresponds to a resonance frequency of TMS (tetramethylsilane). The broken line indicates the position of the chemical shift. The dip at approximately 30 ppm at 3 kbar is a phase-reversed signal arising from the oil pressure medium (Daphne 7373). (**B**) Pressure dependence of the ^{13}C-NMR spin shift (right axis), which is the difference between the averaged value of the two peak positions and a chemical shift of 82 ppm (left axis). (**C**) Pressure dependence of the ^{13}C-NMR spin-lattice relaxation rate $^{13}T_1^{-1}$ at 285 K. (**D**) Comparison between the spin susceptibility χ and $^{13}T_1^{-1}$ in terms of the uniform 1D Heisenberg model. The red closed circles indicate the experimental values obtained for χ and $^{13}T_1^{-1}$ for TTF-CA. The red open circles indicate the values expected for χ ($^{13}T_1^{-1}$) from the uniform 1D Heisenberg model using the experimental values for $^{13}T_1^{-1}$ (χ).

Dynamics of spin solitons

To seek further evidence for mobile solitons, we investigated the frequency dependence of T_1^{-1}, which measures the spectral density of local field fluctuations, $S(\omega)$. The gyromagnetic ratio of the ^{1}H nucleus is four times larger than that of the ^{13}C nucleus, enabling one to reach higher frequencies in experiments; thus, we adopted ^{1}H-NMR for this purpose and carried out measurements for frequencies over a 20-fold range (14 to 300 MHz) at 300 K under 14 kbar in the I_{para} phase. If spin solitons travel in a diffusive manner, $S(\omega)$ should show a frequency dependence characteristic of the spatial dimension for soliton motion, namely, $S(\omega) \propto \omega^{-1/2}$ in 1D, $\propto -\ln\omega$ in 2D, and independent of ω in 3D. In particular, in a 1D-3D crossover regime for quasi-1D systems, $S_{1D\text{-}3D}(\omega)$ is expressed in a form that includes the 1D diffusion rate $D_{||}$ and the 3D cutoff frequency $1/\tau_\perp$(*32*)

$$S_{1D\text{-}3D}(\omega) = \frac{1}{\sqrt{2D_{||}/\tau_\perp}}\left(\frac{1+\sqrt{1+(\omega\tau_\perp)^2}}{1+(\omega\tau_\perp)^2}\right)^{1/2} \quad (3)$$

which yields a $\omega^{-1/2}$ dependence in the 1D regime of $\omega > 1/\tau_\perp$ and approaches a constant, $1/\sqrt{D_{||}/\tau_\perp}$, in the 3D regime of $\omega < 1/\tau_\perp$. Neglecting

the anisotropic part of the hyperfine coupling tensor for simplicity, the contribution of spin diffusion to the relaxation rate is given by $T_1^{-1}{}_{sd} = k_B T(\chi/N_A g^2 \mu_B^2) a_{iso}^2 S(\omega_e)$, where a_{iso} is the isotropic part of the hyperfine coupling tensor, ω_e (= $\gamma_e H$) is the electron Larmor angular frequency (instead of the NMR frequency ω_N), γ_e is the electron gyromagnetic ratio, and g is the electron g-factor (*33*, *34*). As shown in Fig. 4, the behavior of ${}^1T_1^{-1}$ is well fitted by ${}^1T_1^{-1} = k_B T(\chi/N_A g^2 \mu_B^2) {}^1a_{iso}^2 S_{1D\text{-}3D}(\omega_e)$ + constant, with $D_{||} = 5.1 \times 10^{11}$ s^{-1} and $1/\tau_\perp = 5.6 \times 10^{10}$ s^{-1}, using ${}^1a_{iso}$ = −0.39 kOe/μ_B of TTF-BDT(Cu) (*35*). This result signifies that the spin solitons move diffusively at $D_{||} \sim 10^{11}$ s^{-1} along the 1D chains with weak interchain interactions of $1/\tau_\perp \sim 10^{10}$ s^{-1}. The $D_{||}$ value lies in between the two frequency windows of the NQR (10^7 Hz) and infrared (10^{12} Hz) probes, consistent with the dimer-liquid picture. The constant term may derive from longitudinal local field fluctuations through the anisotropic parts of the hyperfine coupling tensor, as discussed in doped *trans*-polyacetylene (*34*). For the origin of the 3D cutoff, exchange interaction between spin solitons on adjacent 1D chains or the hopping of solitons to neighbour chains is conceivable; it is not known at present which mechanism is dominant. The 1D diffusion expressed by $\sqrt{<x(t)^2>} = \sqrt{2D_{||}t}$, where $x(t)$ stands for the soliton position at a time t, leads to the consequence that the solitons travel ~5 donor-acceptor (DA) pairs in time $\tau_\perp$, indicating that the distance between a soliton and an antisoliton running in counter directions varies by ~10 DA pairs in the time period $\tau_\perp$. This distance is comparable with the averaged soliton-antisoliton distance of 25 DA pairs (~$1/n^*$; $n^* = 2n$ is the soliton density per DA pair), reserving another possibility that the cutoff time, ~$\tau_\perp$, is determined by soliton-antisoliton annihilation events. Note that the uniform 1D AF Heisenberg spin system can show diffusive behavior only for $T >> J$ due to the contribution of uniform spin fluctuations ($q \sim 0$) (*36*). The available band parameters for TTF-CA yield a value for J of ~1800 to 3600 K (Supplementary Materials). Thus, in the present case, with T (=300 K) << J, AF fluctuations ($q = \pi$) are dominant and the diffusive behavior is not expected in the uniform 1D AFHM.

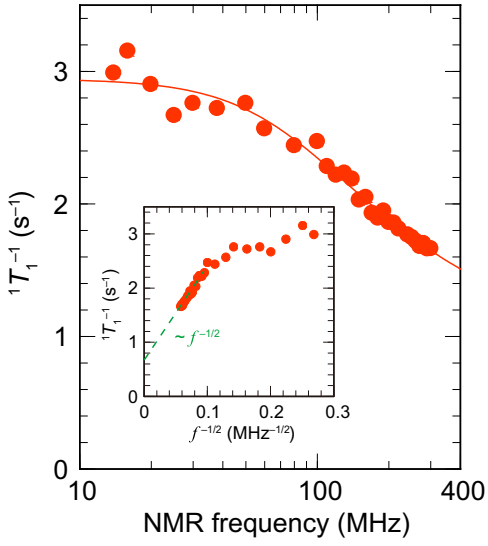

Fig. 4. Frequency dependence of the ^{1}H-NMR relaxation rate. Frequency dependence of ^{1}H-NMR spin-lattice relaxation rate, ${}^1T_1^{-1}$, under 14 kbar at 300 K in the I_{para} phase. The red line is a fit of the form ${}^1T_1^{-1} = k_B T(\chi/N_A g^2 \mu_B^2) {}^1a_{iso}^2 S_{1D\text{-}3D}(\omega_e)$ + constant to the experimental data. Note that ω_e is the Larmor angular frequency of the electron spin. Inset: Plot of ${}^1T_1^{-1}$ against $f^{-1/2}$. A linear extrapolation of the data to $f^{-1/2} = 0$ is indicated by the green broken line.

The present work demonstrates the emergence of solitonic spin excitations from the ferroelectric order. In the vicinity of the NI transition, another type of soliton, namely, the charge soliton, is also expected to emerge (*37*–*41*). It is suggested that the charge and spin solitons carry fractional charges and generate an anomalous charge transport (*37*, *40*, *41*). Note that the anomalous charge transport requires not only charge solitons but also spin solitons; the charge solitons alone cannot sustain steady electrical current. Anomalously high electrical conductivity is reported (*42*). Thus, the present experiments capturing mobile solitons lend support to anomalous charge transport attributed to running solitons along the 1D chains. We expect that solitonic spin and charge excitations in organic charge-transfer complexes bring about unconventional phenomena in various research fields such as thermoelectric transport.

MATERIALS AND METHODS

Sample preparation

The TTF-CA crystals with and without ^{13}C-labeling were prepared by a co-sublimation method; a vacuum-sealed glass tube containing the powdered components in the ends separately was heated with a three-zone temperature-controlled furnace. For ^{13}C-NMR measurements, we synthesized ^{13}C-enriched TTF molecules, in which the central double-bonded carbon atoms were substituted by ^{13}C isotopes (Fig. 1A), according to methods described in the literature (*43*, *44*) with slight modifications from ${}^{13}CS_2$ (ISOTEC, ^{13}C = 99.9 atomic %) as a starting compound. The detail of the scheme is described in fig. S2.

^{1}H-NMR measurements under pressure

We performed ^{1}H-NMR measurements for a TTF-CA single crystal under pressures of up to 17 kbar; the TTF molecule contains four ^{1}H sites. To obtain NMR signals, we used the so-called solid-echo pulse sequence [comb pulse – $(\pi/2)_x$ pulse – $(\pi/2)_y$ pulse]. The NMR spectra for a single crystal of TTF-CA were composed of three or four lines comprising two sets of ^{1}H-^{1}H dipolar splittings (depending on the direction of magnetic field), arising from two differently oriented 1D columns. Except for the measurements of the frequency dependence of ${}^1T_1^{-1}$, the NMR frequency used was ~156.0 MHz under an applied field of 3.66 T. The frequency dependence of ${}^1T_1^{-1}$ was investigated by varying the magnetic field in a range from 0.3 to 7.0 T. The relaxation curve of the nuclear magnetization was fitted by a stretched exponential function ~$\exp(-(t/T_1)^\beta)$, where β is the stretching exponent characterizing the distribution of relaxation rate; in TTF-CA, up to four nonequivalent ^{1}H sites with respect to magnetic field may have different relaxation times. The typical β value was ~0.8 to 0.9. Hydrostatic pressure was applied to the sample using a BeCu clamp-type cell, with DEMNUM oil (solidification pressure of ~10 kbar) used as the hydrogen-free pressure medium. To attain hydrostatic pressures above 10 kbar, we warmed the pressure cell with a heater wound around the cell during the application of pressure for preventing solidification of the oil. We monitored the external pressure while pressurizing the sample at room temperature. The conversion coefficient used to determine the internal pressure from the applied pressure was assumed to be 0.9, which was determined separately by monitoring the resistivity of a manganin wire mounted in the pressure cell. The pressure values quoted in this paper are those determined at room temperature. The temperature variation of the internal pressure of the Daphne oil in the pressurized

and clamped cell was investigated by Murata *et al.* (*45*). As seen in Figs. 1 to 3, important pressure and temperature ranges are above 5 kbar and above 200 K. According to this paper, a drop in pressure upon cooling from room temperature is ~5% at 250 K and ~10% at 200 K for pressures above 5 kbar. The dimerization transition temperatures determined by ${}^{1}T_1^{-1}$ in the present work (red circles in Fig. 1C) nearly coincide with the previous results (white lines in Fig. 1C), although the oil used in the variable-temperature experiments in our study is a different kind of oil, DEMUNUM.

^{13}C-NMR measurements under pressure

^{13}C-NMR measurements were conducted for a ^{13}C-labeled TTF-CA single crystal in a magnetic field H of 8 T applied parallel to the a axis (corresponding to the 1D direction). In this field configuration, all TTF molecules are equivalent against H, and thus, we observed two peaks arising from dipole interactions between the two ^{13}C nuclei on the double-bonded sites. We used a solid-echo pulse sequence to obtain the NMR signals. The spectra shown in Fig. 3A were acquired at the time t_j of $5T_1$ to $10T_1$ after the saturation of nuclear magnetization except for the measurements at 3 kbar; at such a low pressure, T_1 at ^{13}C site was too long to fulfill the ideal condition of $t_j > 5T_1$, and thus, t_j was inevitably set to times comparable to T_1. The spin-lattice relaxation rate ${}^{13}T_1^{-1}$ was determined by fitting the single exponential function to the relaxation curve. To apply hydrostatic pressure to the sample, we used clamp-type pressure cells built using nonmagnetic BeCu with Daphne 7373 as a pressure medium. The conversion coefficient from applied to internal pressures is the same as in the ^{1}H-NMR measurements.

SUPPLEMENTARY MATERIALS

Supplementary material for this article is available at http://advances.sciencemag.org/cgi/content/full/4/11/eaau7725/DC1

Section S1. Deduction of spin susceptibility from the NMR spin shift

Section S2. Hyperfine coupling constants

Section S3. Estimation of the exchange interaction energy J along the 1D axis

Section S4. Temperature dependence of ^{1}H-NMR spectra at 13 kbar

Section S5. Temperature dependence of ^{1}H-NMR relaxation rate

Fig. S1. Molecular frame and principal axes of TTF (X = H) and TMTTF (X = CH_3) molecules.

Fig. S2. Synthetic route for a ^{13}C-enriched TTF molecule.

Fig. S3. Pressure dependence of ^{13}C-NMR spin-lattice relaxation rate at 285 K for a crystal different from the one used in the measurement described in the main text (Fig. 3C).

Fig. S4. Temperature dependence of ^{1}H-NMR spectra at 13 kbar.

Fig. S5. Temperature dependence of ^{1}H-NMR spin-lattice relaxation rate.

References (*46*–*53*)

REFERENCES AND NOTES

1. R. E. Peierls, *Quantum Theory of Solids* (Clarendon Press, 1955).
2. M. C. Cross, D. S. Fisher, A new theory of the spin-Peierls transition with special relevance to the experiments on TTFCuBDT. *Phys. Rev. B.* **19**, 402–419 (1979).
3. Y. M. Bunkov, H. Godfrin, *Topological Defects and the Non-Equilibrium Dynamics of Symmetry Breaking Phase Transitions* (Kluwer Academic Publishers, 2000).
4. S. Brazovskii, in *The Physics of Organic Superconductors and Conductors*, A. Lebed, Ed. (Springer, 2006), pp. 313–355.
5. H. Shirakawa, E. J. Louis, A. G. Macdiarmid, C. K. Chiang, A. J. Heeger, Synthesis of electrically conducting organic polymers : Halogene derivatives of polyacetylene, $(CH)_x$. *J. Chem. Soc. Chem. Commun.*, 578–580 (1977).
6. J. B. Torrance, J. E. Vazquez, J. J. Mayerle, V. Y. Lee, Discovery of a neutral-to-ionic phase transition in organic materials. *Phys. Rev. Lett.* **46**, 253–257 (1981).
7. J. B. Torrance, A. Girlando, J. J. Mayerle, J. I. Crowley, V. Y. Lee, P. Batail, S. J. LaPlaca, Anomalous nature of neutral-to-ionic phase transition in tetrathiafulvalene-chloranil. *Phys. Rev. Lett.* **47**, 1747–1750 (1981).
8. A. Girlando, F. Marzola, C. Pecile, J. B. Torrance, Vibrational spectroscopy of mixed stack organic semiconductors: Neutral and ionic phases of tetrathiafulvalene–chloranil (TTF–CA) charge transfer complex. *J. Chem. Phys.* **79**, 1075–1085 (1983).
9. Y. Tokura, Y. Kane, H. O. S. Tanuma, T. Koda, T. Mitani, G. Saito, Spectroscopic study of the neutral-to-ionic phase transition in TTF-Chloranil. *Mol. Cryst. Liq. Cryst.* **125**, 71–80 (1985).
10. M. Le Cointe, M. H. Lemée-Cailleau, H. Cailleau, B. Toudic, L. Toupet, G. Heger, F. Moussa, P. Schweiss, K. H. Kraft, N. Karl, Symmetry breaking and structural changes at the neutral-to-ionic transition in tetrathiafulvalene-*p*-chloranil. *Phys. Rev. B* **51**, 3374–3386 (1995).
11. K. Kobayashi, S. Horiuchi, R. Kumai, F. Kagawa, Y. Murakami, Y. Tokura, Electronic ferroelectricity in a molecular crystal with large polarization directing antiparallel to ionic displacement. *Phys. Rev. Lett.* **108**, 237601 (2012).
12. T. Mitani, G. Saito, Y. Tokura, T. Koda, Soliton formation at the neutral-to-ionic phase transition in the mixed-stack charge-transfer crystal tetrathiafulvalene-*p*-chloranil. *Phys. Rev. Lett.* **53**, 842–845 (1984).
13. F. Kagawa, S. Horiuchi, H. Matsui, R. Kumai, Y. Onose, T. Hasegawa, Y. Tokura, Electric-field control of solitons in a ferroelectric organic charge-transfer salt. *Phys. Rev. Lett.* **104**, 227602 (2010).
14. M. H. Lemée-Cailleau, M. Le Cointe, H. Cailleau, T. Luty, F. Moussa, J. Roos, D. Brinkmann, B. Toudic, C. Ayache, N. Karl, Thermodynamics of the neutral-to-ionic transition as condensation and crystallization of charge-transfer excitations. *Phys. Rev. Lett.* **79**, 1690–1693 (1997).
15. M. Buron-Le Cointe, E. Collet, B. Toudic, P. Czarnecki, H. Cailleau, Back to the structural and dynamical properties of neutral-ionic phase transitions. *Crystals* **7**, 285 (2017).
16. R. Takehara, K. Sunami, F. Iwase, M. Hosoda, K. Miyagawa, T. Miyamoto, H. Okamoto, K. Kanoda, Revisited phase diagram on charge instability and lattice symmetry breaking in the organic ferroelectric TTF-QCl_4. *Phys. Rev. B* **98**, 054103 (2018).
17. H. Okamoto, T. Koda, Y. Tokura, T. Mitani, G. Saito, Pressure-induced neutral-to-ionic phase transition in organic charge-transfer crystals of tetrathiafulvalene-*p*-benzoquinone derivatives. *Phys. Rev. B* **39**, 10693–10701 (1989).
18. M. Masino, A. Girlando, A. Brillante, Intermediate regime in pressure-induced neutral-ionic transition in tetrathiafulvalene-chloranil. *Phys. Rev. B* **76**, 064114 (2007).
19. Y. Yoshinari, Y. Maniwa, T. Takahashi, K. Mizoguchi, T. Mitani, ^{1}H-NMR studies of neutral-ionic transition in TTF-p-Chloranil. *Synth. Met.* **19**, 521–526 (1987).
20. B. Toudic, J. Gallier, M. Boumaza, H. Cailleau, Proton spin–lattice relaxation study of the neutral-to-ionic transition in TTF-chloranil. *J. Phys. France* **51**, 1671–1678 (1990).
21. H. Matsuzaki, H. Takamatsu, H. Kishida, H. Okamoto, Valence fluctuation and domain-wall dynamics in pressure-induced neutral-to-ionic phase transition of organic charge-transfer crystal. *J. Phys. Soc. Jpn.* **74**, 2925–2928 (2005).
22. C. P. Slichter, *Principles of Magnetic Resonance* (Harper & Row Publishers, 1963).
23. E. Barthel, G. Quirion, P. Wzietek, D. Jérome, J. B. Christensen, M. Jørgensen, K. Bechgaard, NMR in commensurate and incommensurate spin density waves. *Europhys. Lett.* **21**, 87–92 (1993).
24. S. Fujiyama, T. Nakamura, Redistribution of electronic charges in spin-Peierls state in $(TMTTF)_2AsF_6$ observed by ^{13}C NMR. *J. Phys. Soc. Jpn.* **75**, 014705 (2006).
25. A. Girlando, C. Pecile, J. B. Torrance, A key to understanding ionic mixed stacked organic solids: Tetrathiafulvalene-bromanil (TTF-BA). *Solid State Commun.* **54**, 753–759 (1985).
26. F. Kagawa, S. Horiuchi, M. Tokunaga, J. Fujioka, Y. Tokura, Ferroelectricity in a one-dimensional organic quantum magnet. *Nat. Phys.* **6**, 169–172 (2010).
27. J. C. Bonner, M. E. Fisher, Linear magnetic chains with anisotropic coupling. *Phys. Rev.* **135**, A640–A658 (1964).
28. W. E. Estes, D. P. Gavel, W. E. Hatfield, D. J. Hodgson, Magnetic and structural characterization of dibromo- and dichlorobis(thiazole)copper(II). *Inorg. Chem.* **17**, 1415–1421 (1978).
29. S. Sachdev, NMR relaxation in half-integer antiferromagnetic spin chains. *Phys. Rev. B* **50**, 13006–13008 (1994).
30. M. Takigawa, N. Motoyama, H. Eisaki, S. Uchida, Dynamics in the $S = 1/2$ one-dimensional antiferromagnet Sr_2CuO_3 via ^{63}Cu NMR. *Phys. Rev. Lett.* **76**, 4612–4615 (1996).
31. B. Salameh, S. Yasin, M. Dumm, G. Untereiner, L. Montgomery, M. Dressel, Spin dynamics of the organic linear chain compounds $(TMTTF)_2X$ (X = SbF_6, AsF_6, BF_4, ReO_4, and SCN). *Phys. Rev. B* **83**, 205126 (2011).
32. K. Mizoguchi, K. Kume, H. Shirakawa, Frequency dependence of electron spin–lattice relaxation rate at 5–450 MHz in pristine trans-polyacetylene—New evidence of one dimensional diffusive motion of electron spin (neutral soliton). *Solid State Commun.* **50**, 213–218 (1984).
33. F. Devreux, Nuclear relaxation in one-dimensional Hubbard systems. *Phys. Rev. B* **13**, 4651–4657 (1976).
34. M. Nechtschein, F. Devreux, R. L. Greene, T. C. Clarke, G. B. Street, One-dimensional spin diffusion in polyacetylene, $(CH)_x$. *Phys. Rev. Lett.* **44**, 356–359 (1980).
35. F. Devreux, C. Jeandey, M. Nechtschein, J. M. Fabre, L. Giral, Electron-proton couplings and local susceptibilities in TTF and TCNQ salts. *J. Phys. France* **40**, 671–677 (1979).
36. J. Kikuchi, N. Kurata, K. Motoya, T. Yamauchi, Y. Ueda, Spin diffusion in the $S = 1/2$ quasi one-dimensional antiferromagnet α-$VO(PO_3)_2$ via ^{31}P NMR. *J. Phys. Soc. Jpn.* **70**, 2765–2773 (2001).

37. N. Nagaosa, Theory of neutral-ionic transition in organic crystals. III. Effect of the electron-lattice interaction. *J. Phys. Soc. Jpn.* **55**, 2754–2764 (1986).
38. M. Buron-Le Cointe, M. H. Lemée-Cailleau, H. Cailleau, S. Ravy, J. F. Bérar, S. Rouzière, E. Elkaïm, E. Collet, One-dimensional fluctuating nanodomains in the charge-transfer molecular system TTF-CA and their first-order crystallization. *Phys. Rev. Lett.* **96**, 205503 (2006).
39. Z. G. Soos, A. Painelli, Metastable domains and potential energy surfaces in organic charge-transfer salts with neutral-ionic phase transitions. *Phys. Rev. B* **75**, 155119 (2007).
40. H. Fukuyama, M. Ogata, Solitons in the crossover between band insulator and Mott insulator: Application to TTF-Chloranil under pressure. *J. Phys. Soc. Jpn.* **85**, 023702 (2016).
41. M. Tsuchiizu, H. Yoshioka, H. Seo, Phase competition, solitons, and domain walls in neutral-ionic transition systems. *J. Phys. Soc. Jpn.* **85**, 104705 (2016).
42. R. Takehara, K. Miyagawa, K. Kanoda, T. Miyamoto, H. Matsuzaki, H. Okamoto, H. Taniguchi, K. Matsubayashi, Y. Uwatoko, Electron transport in TTF-CA under high pressures. *Physica B* **460**, 83–87 (2015).
43. Y. Ueno, A. Nakayama, M. Okawara, A convenient synthesis of 1,3-dithiole-2-thione and related compounds. *Synthesis* **40**, 277–278 (1975).
44. F. Wudl, M. L. Kaplan, E. J. Hufnagel, E. W. Southwick Jr., A convenient synthesis of 1,4,5,8-tetrahydro-1,4,5,8-tetrathiafulvalene. *J. Org. Chem.* **39**, 3608–3609 (1974).
45. K. Murata, H. Yoshino, H. O. Yadav, Y. Honda, N. Shirakawa, Pt resistor thermometry and pressure calibration in a clamped pressure cell with the medium, Daphne 7373. *Rev. Sci. Instrum.* **68**, 2490–2493 (1997).
46. C. Katan, First-principles study of the structures and vibrational frequencies for Tetrathiafulvalene TTF and TTF-d_4 in different oxidation states. *J. Phys. Chem. A* **103**, 1407–1413 (1999).
47. P. Delhaes, C. Coulon, J. Amiell, S. Flandrois, E. Toreilles, J. M. Fabre, L. Giral, Physical properties of one dimensional conductors. *Mol. Cryst. Liq. Cryst.* **50**, 43–58 (1979).
48. L. Cavara, F. Gerson, D. O. Cowan, K. Lerstrup, An ESR study of the radical cations of tetrathiafulvalene (TTF) and electron donors containing the TTF moiety. *Helv. Chim. Acta* **69**, 141–151 (1986).
49. C. S. Jacobsen, J. B. Torrance, Behavior of charge-transfer absorption upon passing through the neutral-ionic phase transition. *J. Chem. Phys.* **78**, 112–115 (1983).
50. V. Oison, C. Katan, P. Rabiller, M. Souhassou, C. Koenig, Neutral-ionic phase transition: A thorough ab initio study of TTF-CA. *Phys. Rev. B* **67**, 035120 (2003).
51. Y. Tokura, T. Koda, T. Mitani, G. Saito, Neutral-to-ionic transition in tetrathiafulvalene-*p*-chloranil as investigated by optical reflection spectra. *Solid State Commun.* **43**, 757–760 (1982).
52. N. Nagaosa, J. Takimoto, Theory of neutral-ionic transition in organic crystals. II. Effect of the intersite Coulomb interaction. *J. Phys. Soc. Jpn.* **55**, 2745–2754 (1986).
53. R. M. Metzger, J. B. Torrance, Role of the madelung energy in the neutral-ionic phase transition of tetrathiafulvalene chloranil. *J. Am. Chem. Soc.* **107**, 117–121 (1985).

Acknowledgments: We thank H. Fukuyama, T. Takahashi, M. Ogata, T. Hasegawa, and R. Takehara for critical discussions. **Funding:** This work was supported by the JSPS Grant-in-Aids for Scientific Research (S) (grant nos. JP25220709, JP18H05225, and JP16H06346) and for Scientific Research (C) (grant no. JP17K05532) and by CREST (grant no. JPMJCR1661), Japan Science and Technology Agency. **Author contributions:** K.S., T.N., and K.M. performed the NMR measurements. R.K. synthesized the ^{13}C-enriched TTF molecules. S.H., T.M., and H.O. prepared the TTF-CA single crystals. K.S. wrote the manuscript with the assistance of K.M. and K.K. K.S., K.M., and K.K. designed the experiments. All authors discussed the results and commented on the manuscript. This project is headed by K.K. **Competing interests:** The authors declare that they have no competing interests. **Data and materials availability:** All data needed to evaluate the conclusions in the paper are present in the paper and/or the Supplementary Materials. Additional data related to this paper may be requested from the authors. Correspondence and requests for materials should be addressed to K.S. or K.K.

Submitted 13 July 2018
Accepted 30 October 2018
Published 30 November 2018
10.1126/sciadv.aau7725

Citation: K. Sunami, T. Nishikawa, K. Miyagawa, S. Horiuchi, R. Kato, T. Miyamoto, H. Okamoto, K. Kanoda, Evidence for solitonic spin excitations from a charge-lattice–coupled ferroelectric order. *Sci. Adv.* **4**, eaau7725 (2018).